A critical role for the right fronto-insular cortex in switching between central-executive and default-mode networks

Devarajan Sridharan*†‡, Daniel J. Levitin§, and Vinod Menon*†‡¶

*Department of Psychiatry and Behavioral Sciences, †Program in Neuroscience and ¶Neuroscience Institute at Stanford, Stanford University School of Medicine, Stanford, CA 94305 and §Department of Psychology, School of Computer Science and Program in Behavioural Neuroscience, McGill University, 1205 Avenue Penfield, Montreal, QC, Canada H3A 1B1

Edited by Marcus E. Raichle, Washington University School of Medicine, St. Louis, MO, and approved June 20, 2008 (received for review January 1, 2008)

Cognitively demanding tasks that evoke activation in the brain's central-executive network (CEN) have been consistently shown to evoke decreased activation (deactivation) in the default-mode network (DMN). The neural mechanisms underlying this switch between activation and deactivation of large-scale brain networks remain completely unknown. Here, we use functional magnetic resonance imaging (fMRI) to investigate the mechanisms underlying switching of brain networks in three different experiments. We first examined this switching process in an auditory event segmentation task. We observed significant activation of the CEN and deactivation of the DMN, along with activation of a third network comprising the right fronto-insular cortex (rFIC) and anterior cingulate cortex (ACC), when participants perceived salient auditory event boundaries. Using chronometric techniques and Granger causality analysis, we show that the rFIC-ACC network, and the rFIC, in particular, plays a critical and causal role in switching between the CEN and the DMN. We replicated this causal connectivity pattern in two additional experiments: (*i*) a visual attention ''oddball'' task and (*ii*) a task-free resting state. These results indicate that the rFIC is likely to play a major role in switching between distinct brain networks across task paradigms and stimulus modalities. Our findings have important implications for a unified view of network mechanisms underlying both exogenous and endogenous cognitive control.

brain networks | cognitive control | insula | attention | prefrontal cortex

One distinguishing feature of the human brain, compared with brains lower on the phylogenetic ladder, is the amount of cognitive control available for selecting, switching, and attending to salient events in the environment. Recent research suggests that the human brain is intrinsically organized into distinct functional networks that support these processes (1–4). Analysis of resting-state functional connectivity, using both model-based and model-free approaches, has suggested the existence of at least three canonical networks: (*i*) a central-executive network (CEN), whose key nodes include the dorsolateral prefrontal cortex (DLPFC), and posterior parietal cortex (PPC); (*ii*) the default-mode network (DMN), which includes the ventromedial prefrontal cortex (VMPFC) and posterior cingulate cortex (PCC); and (*iii*) a salience network (SN), which includes the ventrolateral prefrontal cortex (VLPFC) and anterior insula (jointly referred to as the fronto-insular cortex; FIC) and the anterior cingulate cortex (ACC) (1, 2, 4, 5). During the performance of cognitively demanding tasks, the CEN and SN typically show increases in activation whereas the DMN shows decreases in activation (1, 2, 6). However, what remains unknown is the crucial issue of how the operation of these networks, identified in the resting state, relate to their function during cognitive information processing. Furthermore, the cognitive control mechanisms that mediate concurrent activation and deactivation within these large-scale brain networks during task performance are poorly understood.

In a recent meta-analysis, Dosenbach and colleagues hypothesized that several brain regions that overlap with the CEN and SN are important for multiple cognitive control functions, including initiation, maintenance, and adjustment of attention (7). However, no studies to date have directly assessed the temporal dynamics and causal interactions of specific nodes within the CEN, SN, and DMN. Converging evidence from a number of brain imaging studies across several task domains suggests that the FIC and ACC nodes of the SN, in particular, respond to the degree of subjective salience, whether cognitive, homeostatic, or emotional (4, 8–11). The CEN, on the other hand, is critical for the active maintenance and manipulation of information in working memory, and for judgment and decision making in the context of goal directed behavior (12–18). We therefore hypothesized a key role for the SN in the hierarchical initiation of cognitive control signals, specifically with respect to activation and deactivation in the CEN and DMN, and the dynamics of switching between these two networks.

We used three functional magnetic resonance imaging (fMRI) experiments to examine the interaction between the SN, CEN, and DMN, with particular interest in the role of the FIC/ACC in regulating these networks. In the first experiment, we scanned 18 participants as they listened with focused attention to classical music symphonies inside the scanner. We analyzed brain responses during the occurrence of ''movement transitions:'' salient, orienting events arising from transitions between adjacent ''movements'' in the music (19). To specifically elucidate the role of the FIC in driving network changes, we used chronometry and Granger Causality Analysis (GCA), to provide information about the dynamics and directionality of signaling in cortical circuits (20–22).

In the second experiment, we investigated the generality of network switching mechanisms involving the FIC by examining brain responses elicited during a visual ''oddball'' attention task (23). A third experiment examined whether the network switching mechanism could be observed during task-free resting state where there was no overt task and no behavioral response (4). Our motivation for examining the resting-state fMRI data was the recent finding, based on computer simulation of large-scale brain networks, that even in the absence of external stimuli, certain nodes can regulate other nodes and function as hubs (24).

Author contributions: V.M. designed research; D.S., D.J.L., and V.M. performed research; D.S. analyzed data; and D.S. and V.M. wrote the paper.

The authors declare no conflict of interest.

This article is a PNAS Direct Submission.

‡To whom correspondence may be addressed at: Program in Neuroscience and Department of Psychiatry and Behavioral Sciences, Stanford University School of Medicine, 780 Welch Road, Room 201, Stanford, CA 94305-5778. E-mail: dsridhar@stanford.edu or menon@stanford.edu.

This article contains supporting information online at www.pnas.org/cgi/content/full/0800005105/DCSupplemental.

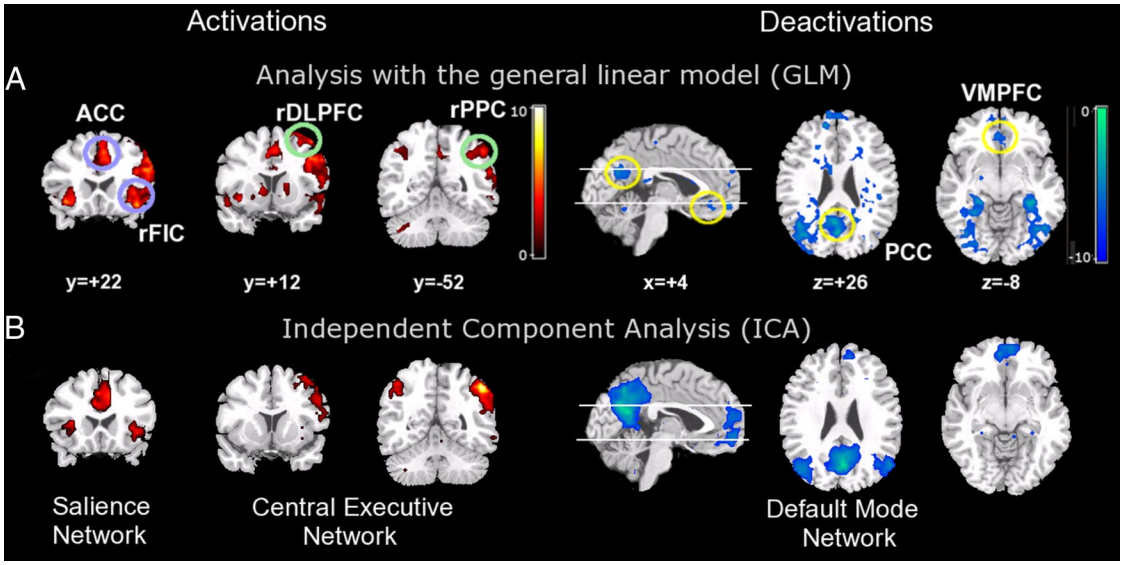

Fig. 1. Activations in the Central-Executive and Salience Networks and deactivations in the Default-Mode Network during auditory event transitions. (*A*) Analysis with the General Linear Model (GLM) revealed regional activations (*Left*) in the right hemispheric FIC and ACC (blue circles); DLPFC and PPC (green circles) (coronal sections at y = +22, +12 and −52 mm) and deactivations (*Right*) in the VMPFC and PCC (sagittal section at x = +4 mm and axial sections at z = +26 and −8 mm, yellow circles) during event transitions. The scale for t-scores is shown along side. Activations height and extent thresholded at the $P < 0.01$ level (corrected). (*B*) *Independent Component Analysis* (ICA, a model-free analysis technique) provided converging evidence for spatially independent and distinct networks. From left to right: Salience Network (rFIC and ACC), Central-Executive Network (rDLPFC and rPPC), and Default-Mode Network (VMPFC and PCC). Activations height and extent thresholded at the $P < 0.001$ level (uncorrected). The ICA prunes out extraneous activation and deactivation clusters visible in the GLM analysis to reveal brain regions that constitute independent and tightly coupled networks.

Our aim was to test the hypothesis that common network switching mechanisms apply across tasks with varying cognitive demands and differing stimulus modalities. If confirmed, our findings would provide insights into fundamental control mechanisms in the human brain.

Results

We describe findings from Experiment 1 in the first three sections. Convergent findings from Experiments 2 and 3 are described subsequently.

Activation of CEN and SN, and Deactivation of DMN During Auditory Event Segmentation. As reported previously (19), we found robust right-lateralized activation in the DLPFC, PPC, and FIC during "movement transitions" in the auditory event segmentation task. Here, we extend these findings to characterize network-specific responses in the CEN, DMN, and SN. Activations in the CEN and SN were found to be accompanied by robust deactivation in the DMN at the movement transition [Fig. 1*A* and General Linear Model Analysis in supporting information (SI) *Materials and Methods*]. To further confirm that these regions constitute coherent networks, rather than isolated regional responses, we performed independent component analysis (ICA) on the task data, which revealed the existence of statistically independent CEN, SN, and DMN (Fig. 1*B*, see also Table S1) [ICA is a model-free analysis technique that produces a set of spatially independent components and associated time courses for each subject (25)]. In the following two sections, we examine the putative causal mechanisms involved in switching between activation and deactivation in the context of the three networks, identified above, using a combination of mental chronometry and GCA (21, 22).

Latency Analysis Reveals Early Activation of the rFIC Relative to the CEN and DMN. First, we identified differences in the latency of the event-related fMRI responses across the entire brain using the method developed by Henson and colleagues (26). Briefly, this method provides a way to estimate the peak latency of the BOLD response at each voxel using the ratio of the derivative to canonical parameter estimates (see *SI Materials and Methods* for details). This analysis revealed that the event-related fMRI signal in the right FIC (rFIC) and ACC peaks earlier compared to the signal in the nodes of the CEN and DMN, indicating that the neural responses in the rFIC and ACC precede the CEN and DMN (see Fig. S1 and Table S2). To provide converging quantitative evidence, we estimated the onset latency of the blood oxygen level dependent (BOLD) response in these regions using the method of Sterzer and Kleinschmidt (27). Previous studies have used differences in the onset latency of the BOLD response as a measure of the difference in onset of the underlying neural activity (20, 21, 27). We first defined regions of interest (ROIs) in six key nodes of the SN, CEN, and DMN based on the peaks of the ICA clusters (see *Materials and Methods*); all subsequent analyses was confined to these six canonical nodes of the SN, CEN, and DMN (see also *SI Text* for a discussion on the choice of regions of interest and control analyses on regions not included in the main analysis). We extracted the mean time-course in each of these six nodes, and used a sixth-order Fourier model to fit the event related BOLD response for each subject and event, and averaged the fitted responses across events and subjects (see Fig. S2). Onset latencies were then computed as the time point at which the slope of the fitted response reached 10% of its maximum positive (or negative) slope in the initial ascending (or descending) segment. We found that the rFIC onsets significantly earlier than all of the nodes in the CEN and DMN (two-sample *t*-test, $q < 0.05$; FDR correction for multiple comparisons) (Fig. 2, see also Table S3). These results confirm that activity in the rFIC onsets earlier compared to the activation in the CEN nodes, and deactivation in the DMN nodes.

GCA Reveals that the rFIC Is a Causal Outflow Hub at the Junction of the CEN and DMN. Finally, to elucidate the dynamic interactions between the three networks we applied GCA. Briefly, GCA detects causal interactions between brain regions by assessing the

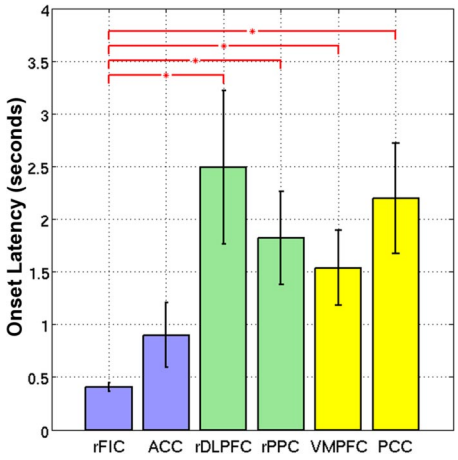

Fig. 2. Onset latencies of the event-related responses in the six key nodes of the SN (blue bars), CEN (green bars) and DMN (yellow bars) in the auditory event segmentation task. The rFIC onset significantly earlier than each of the nodes in the CEN and DMN (two-sample *t*-test, q <0.05, indicated by (*), FDR corrected for multiple comparisons). Error bars denote standard error of the mean (SEM) across subjects.

predictability of signal changes in one brain region based on the time-course of responses in another brain region (28). We performed GCA using a bivariate model (22) on the time-courses extracted from the six key regions used in the onset latency analysis. We used bootstrap techniques (29) to create null distributions of influence terms (*F*-values) and their differences (22). A causal connectivity graph was constructed using the thickness of connecting arrows to indicate the strengths of the causal influences (Fig. 3*A*, "raw" *F*-values normalized by the maximum *F*-value; raw *F*-values reported in Table S4). Only links that showed significant directed connectivity (influence terms) at the group-level (Mann-Whitney *U* test, $P < 0.01$; Bonferroni corrected for multiple comparisons) are shown (gray arrows, Fig. 3*A*); a subset of these links that showed a dominant direction of influence (difference of influence terms) are highlighted in red in the same figure (Mann-Whitney *U* test, $P < 0.05$, FDR corrected links shown in Table S4) (see *SI Materials and Methods* for details). GCA on the time-courses extracted from the key regions revealed statistically significant direct or indirect causal influences from the rFIC to all of the regions in the CEN and DMN (Fig. 3*A*). To quantify the causal interactions of each node of the network, we performed network analyses on key graph metrics (see *Materials and Methods*), and constructed a distribution of these metrics, across subjects (for each node). Network analysis on the causal flow network identified with GCA revealed that the rFIC had the highest number of causal outflow connections (out-degree), the lowest number of causal inflow connections (in-degree), and the shortest path length among all regions (means and standard errors of these metrics are reported in Table S5*A*). The rFIC also had a significantly higher net causal outflow (out-in degree) than all of the nodes of the CEN and DMN (two-sample *t* test, $P < 0.05$). Differences in (out-in) degree between the rFIC and the rDLPFC, rPPC, and PCC remained significant after FDR correction for multiple comparisons ($q < 0.05$) (Fig. 4*A*). Similarly, the rFIC had a significantly

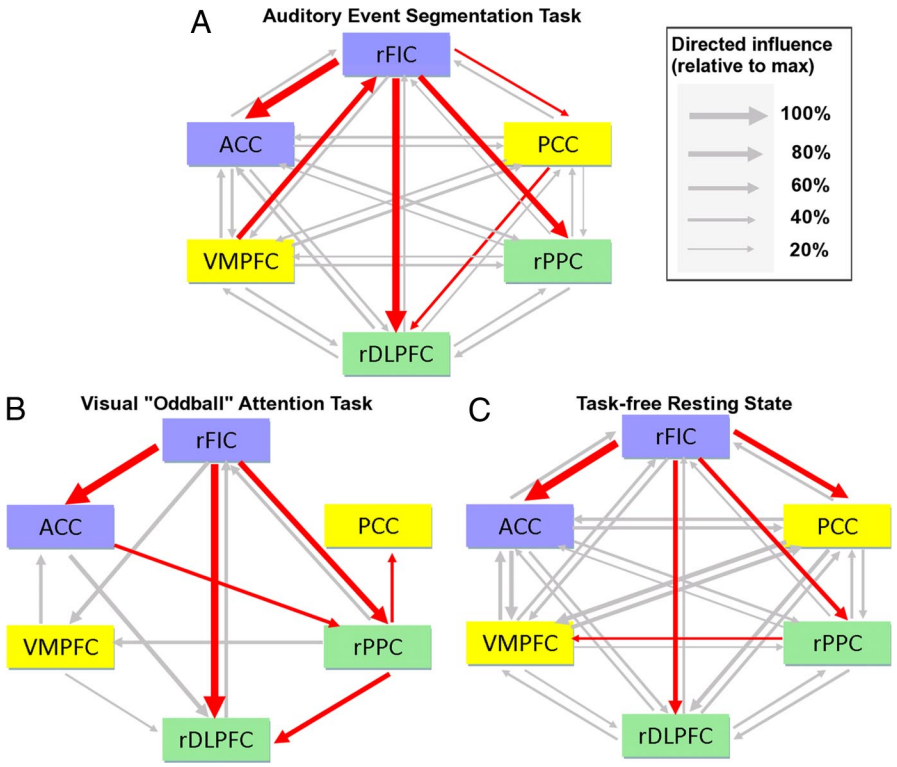

Fig. 3. Granger causality analysis (GCA) of the six key nodes of the Salience (blue nodes), Central-Executive (green nodes) and Default-Mode (yellow nodes) networks during (*A*) auditory event segmentation, (*B*) visual oddball attention task, and (*C*) task-free resting state. GCA revealed significant causal outflow from the rFIC across tasks and stimulus modalities. In each subfigure, the thickness of the connecting arrows between two regions corresponds to the strength of directed connection (*F*-value) normalized by the maximum *F*-value between any pair of regions for that task (''raw'' *F*-values reported in Table S4). Only links that showed significant directed connectivity at the group-level (Mann-Whitney *U* test, $P < 0.01$; Bonferroni corrected for multiple comparisons) are shown (gray arrows); a subset of these links that showed a dominant directional influence (difference of influence term) are highlighted in red (Mann-Whitney *U* test, $P < 0.05$).

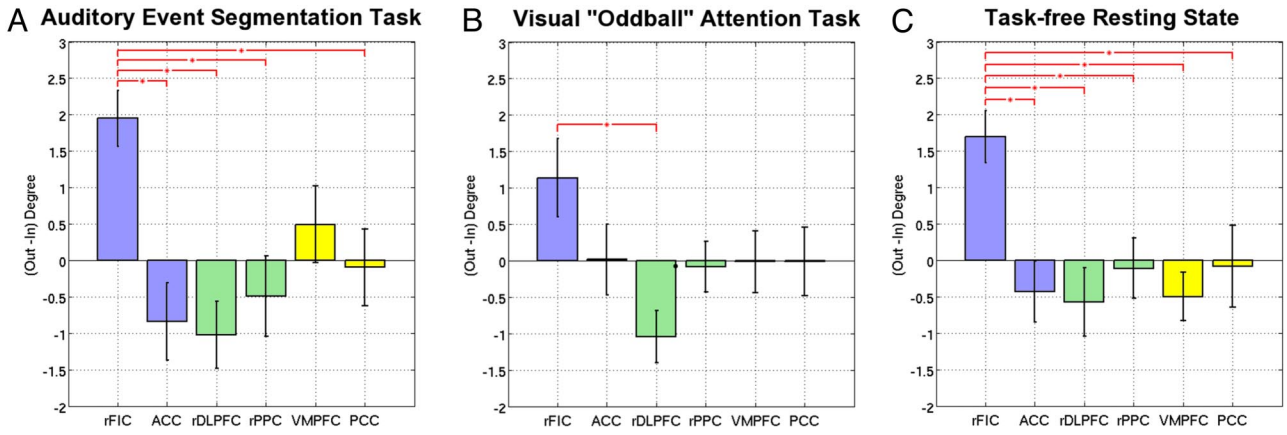

Fig. 4. Net Granger causal outflow (out-in degree) of the key nodes of the Salience, Central-Executive, and Default-Mode Networks in the three experiments. Comparison of the net causal outflow (out-in degree) for the six key nodes of the Salience, Central-Executive, and Default-Mode networks as assessed by Granger causality analysis revealed that the rFIC has a significantly higher net causal outflow than the CEN and DMN regions across tasks (conventions as in Fig. 2). Specifically, the rFIC had a significantly higher net causal outflow than almost all of the other CEN and DMN regions for the auditory segmentation and resting-state tasks, and the rDLPFC for the visual oddball task (two-sample *t*-test, $q < 0.05$, indicated by (*), FDR corrected for multiple comparisons).

shorter path length than all of the other regions except the VMPFC (*t* test, $P < 0.05$); however, these differences did not remain significant after multiple comparison correction (data not shown). These results suggest that the rFIC is an outflow hub at the junction of the CEN and DMN.

Converging Evidence from Two Additional fMRI Experiments. To provide converging evidence for the rFIC as a causal outflow hub, we analyzed fMRI data from two other experiments using the same GCA and network analyses methods described above: (*i*) a visual "oddball" attention experiment, and (*ii*) a task-free resting state experiment (see also *SI Materials and Methods*). We found a pattern of significant causal outflow from the rFIC that was strikingly similar to the auditory event segmentation experiment (Fig. 3 *B* and *C*). We then constructed network metrics for these tasks using a procedure identical to the one used for the auditory segmentation task. In each case, the rFIC had the highest out-in degree and the shortest path length (Table S5 *B* and *C*). Again, the rFIC again had a significantly higher net causal outflow than several of the other nodes of the CEN and DMN (Fig. 4 *B* and *C*). Specifically, the rFIC had a significantly higher (out-in) degree than all of the other CEN and DMN nodes in the resting state, and the rDLPFC in the visual oddball task (two-sample *t*-test, $q < 0.05$, FDR correction for multiple comparisons). These converging results indicate that that the rFIC is a critical, causal outflow hub across task paradigms and stimulus modalities.

Discussion

ICA revealed the existence of statistically independent CEN, DMN, and SN during task performance, extending our recent discovery of similar networks in task-free, resting-state, conditions (4). Our analysis indicates that the rFIC, a key node of the SN, plays a critical and causal role in switching between the CEN and the DMN (we use the term "causal" here, and in the following sections in the sense implied by, and consistent with, latency analysis, GCA and network analysis). The striking similarity of significant causal outflow from the rFIC across tasks, involving different stimulus modalities, indicates a general role for the rFIC in switching between two key brain networks. Furthermore, our replication of this effect in the task-free resting state suggests that the rFIC is a network hub that can also initiate spontaneous switching between the CEN and DMN (24). Our findings help to provide a more unified perspective on exogenous and endogenous mechanisms underlying cognitive control.

In the *SI Discussion*, we suggest that these interactions are the result of neural, rather than vascular processes. Here, we focus on the neurobiological implications of our findings in the context of the three networks that we set out to examine; analyses of several other control regions (including the sensory and association cortices) that further clarify the crucial role of the FIC in the switching process are discussed in the *SI Text*.

FIC-ACC Network Is Neuroanatomically Uniquely Positioned to Generate Control Signals. In primates, anatomical studies have revealed that the insular cortex is reciprocally connected to multiple sensory, motor, limbic, and association areas of the brain (30, 31). The FIC and ACC themselves share significant topographic reciprocal connectivity and form an anatomically tightly coupled network ideally placed to integrate information from several brain regions (9, 10, 32). Indeed, analysis of the auditory and visual experiments in our study found coactivation of these regions during task performance, as in many other studies involving cognitively demanding tasks (7). Previous neurophysiological and brain imaging studies have shown that the FIC-ACC complex moderates arousal during cognitively demanding tasks and that the rFIC, in particular, plays a critical role in the interoceptive awareness of both stimulus-induced and stimulus-independent changes in homeostatic states (9, 10). Furthermore, the FIC and ACC share a unique feature at the neuronal level: The human FIC-ACC network has a specialized class of neurons with distinctive anatomical and functional features that might facilitate the network switching process that we report here. The von Economo neurons (VENs) are specialized neurons exclusively localized to the FIC and ACC (33). Based on the dendritic architecture of the VENs, Allman and colleagues have proposed that "the function of the VENs may be to provide a rapid relay to other parts of the brain of a simple signal derived from information processed within FI and ACC." (34). We propose that the VENs may, therefore, constitute the neuronal basis of control signals generated by the FIC and ACC in our study. Taken together, these findings suggest that the FIC and ACC, anchored within the SN, are uniquely positioned to initiate control signals that activate the CEN and deactivate the DMN.

Differential Roles of the rFIC, ACC, and Lateral Prefrontal Cortex in Initiating Control Signals. Many previous studies of attentional and cognitive control have reported coactivation of the FIC and

ACC (7, 23, 35, 36). The differential role of each of these regions has been poorly understood (37) as few studies have used chronometric techniques or causal analyses to dissociate the temporal and network dynamics of responses in these regions. We found that although onset latencies in the rFIC and ACC did not differ significantly, as might be expected from their being part of the same (salience) network, the FIC did have a powerful causal influence on the ACC (and correspondingly, higher net causal outflow than the ACC) in all three datasets (Figs. 3 and 4). Even under conditions in which the ACC plays an important role in cognitive control (23, 36), the rFIC may generate the signals to trigger hierarchical control and previous studies, including ours, may have missed detecting these effects. Our data further suggest that when the ACC is dysfunctional (38, 39), the FIC is well positioned to trigger alternate cognitive control mechanisms via the CEN. Our findings therefore help to clarify an important controversy regarding the primacy and uniqueness of control signals in the prefrontal cortex (39).

Brain regions in the right inferior frontal cortex, surrounding the FIC, have been implicated in a wide range of cognitive control mechanisms (40–42). For example, many of the paradigms involving response inhibition and inhibitory control have focused on ventrolateral regions (primarily within BA 47 and 45) within the right inferior frontal gyrus (43). However, the specific role of the right FIC has been less well studied perhaps because it is usually coactive with the lateral prefrontal cortex. A notable exception is a study by Dosenbach *et al.* (44) who used resting-state fMRI blocks, interspersed between task blocks, and graph theoretical analysis to underscore the distinctiveness of the FIC and its connectivity with the ACC. Further, a recent lesion study in humans has shown that the rFIC has an important role in cognitive control related to task switching. Using an oculomotor-switching task Hodgson and colleagues (45) showed that patients with lesions in the anterior rFIC were the most impaired in altering their behavior in accordance with the changing rules of the task. In normal healthy adults, functional brain imaging studies have suggested that the FIC and the ACC are together involved in a variety of cognitive control processes, including conflict and error monitoring, interference resolution, and response selection (23, 36, 40, 46–48). We hypothesize that in all these cases, the rFIC enables task-related information processing by initiating appropriate control signals to engage the ACC and the CEN. Our findings are inconsistent with the suggestion that the FIC-ACC provides stable 'set-maintenance' over entire task epochs whereas the fronto-parietal component initiates and adjusts control (49). In our view, it is the FIC-ACC-centered SN network that initiates key control signals in response to salient stimuli or events. As the lesion study by Hodgson and colleagues illustrates so dramatically, failure to generate these signals can have severe consequences for behavior. Our findings do not, however, preclude the possibility that after the FIC initiates changes in intra- and inter-network activity the CEN may carry out top-down important control functions either on its own or in association with the SN.

Our findings help to synthesize these and other extant findings in the literature into a common network dynamical framework and they suggest a causal, and potentially critical, role for the rFIC in cognitive control. We propose that one fundamental mechanism underlying such control is a transient signal from the rFIC, which engages the brain's attentional, working memory and higher-order control processes while disengaging other systems that are not task-relevant. We predict that disruptions to these processes may constitute a key aspect of psychopathology in several neurological and psychiatric disorders, including frontotemporal dementia, autism, and anxiety disorders (34, 50, 51). More generally, our study illustrates the power of a unified network approach—wherein we first specify intrinsic brain networks and then analyze interactions among anatomically discrete regions within these networks during cognitive information processing—for understanding fundamental aspects of human brain function and dysfunction.

Materials and Methods

Experimental Design. We used data from three different experiments. The first experiment involved auditory event segmentation and detection of salient event boundaries in passages of music by the Baroque composer William Boyce. Eighteen right-handed participants (19–27 years of age, 8 females) with little or no musical training participated in the experiment. Participants listened to stimuli with focused attention inside the scanner over noise-reducing headphones. A follow-up behavioral study conducted outside the scanner ensured that subjects could accurately detect the occurrence of movement transitions when these occurred in the stimulus. Further details can be found in Sridharan *et al.* (19). The second experiment involved a visual oddball task. Thirteen subjects (24 $\pm$ 4.5 years of age, 8 females) participated in the experiment. Two hundred visual stimuli were presented for 150 ms with a 2,000-ms interval between stimulus onsets. Visual stimuli consisted of colored circles (either blue or green) and the frequency of the colored circles was counterbalanced across subjects (such that for half of them, green was the infrequent stimulus). Further details can be found in Crottaz-Herbette and Menon (23). The third experiment involved an eight minute resting state scan in which twenty-two subjects participated (19–21 years of age, 11 females). Subjects were instructed to rest while keeping their eyes closed and were requested to avoid moving during the scan (4).

fMRI Acquisition, analysis with the General Linear Model (GLM), Independent Component Analysis (ICA), the Calculation of Peak and Onset Latency differences, and Granger Causality Analysis (GCA) followed the procedure reported in a previously published experiment (19). Details can be found in the *SI*. Here, we describe methods specifically related to network analysis of causal interactions.

Region of Interest (ROI) Definition and Time Series Extraction. ROI analysis was performed using the Marsbar software package (http://marsbar.sourceforge.net). Spherical ROIs were defined as the sets of voxels contained in 6–10-mm spheres centered on the peaks of activation clusters obtained from the ICA analysis (Table S1). These same ROIs were used throughout all of the subsequent analyses (onset latency, GCA, and network analyses). The mean time course in each ROI was extracted by averaging the time courses of all of the voxels contained in the ROI.

Granger Causality Analysis. GCA was performed using the Causal Connectivity Toolbox (52), with modifications based on the methods proposed by Roebroeck *et al.* (22). GCA was performed on the timeseries extracted from ROIs to test for causal influences between ROIs taken pairwise using the difference of influence term ($F_{x\to y} - F_{y\to x}$) (22). We performed statistical inference on the causal connections using bootstrap analysis: An empirical null distribution of the difference of influence terms was estimated using block-randomized time series (22). For each subject, dominant (difference of influence) connections that passed a $P = 0.05$ significance level (bootstrap threshold) were used for computing the network metrics described next. For details on the construction of the causal connectivity graph (Fig. 3) refer to *SI Materials and Methods*.

Network Analysis. To describe the interactions between brain regions in the causal network generated by GCA, we list the definition of the following metrics used in traditional graph-theoretic analyses (52):

a) Out-degree: Number of causal outflow connections from a node in the network to any other node.

b) In-degree: Number of causal in-flow connections to a node in the network from any other node

c) (Out − In) degree: Difference between out-degree and in-degree is a measure of the net causal outflow from a node.

d) Path length: Shortest path from a node to every other node in the network (normalized by the number of nodes minus one). Shorter path lengths indicate a more strongly interconnected or ''hub-like'' node.

For the present analysis, we constructed a distribution of these metrics, across subjects, for each node of the network. The mean value of these metrics (and their standard errors) across subjects are reported in Table S5. Path length was computed using Dijkstra's shortest path algorithm (53). A two-sample *t*-test was then applied on two key network metrics, the (out-in) degree and the path length, with FDR correction for multiple comparisons, to identify those nodes whose network metrics were significantly different from the other nodes.

ACKNOWLEDGMENTS. We thank Mike Greicius for useful discussions and Elena Rykhlevskaia and Catie Chang for their comments on a preliminary draft of this manuscript. We acknowledge two anonymous reviewers for their insightful comments and suggestions. This research was supported by a Stanford Graduate Fellowship to D.S. and by grants from the Natural Sciences and Engineering Research Council of Canada to D.J.L., the National Science Foundation (BCS-0449927) to V.M. and D.J.L., and the National Institutes of Health (HD047520, NS058899) to V.M.

1. Greicius MD, Krasnow B, Reiss AL, Menon V (2003) Functional connectivity in the resting brain: A network analysis of the default mode hypothesis. *Proc Natl Acad Sci USA* 100:253–258.
2. Fox MD, Corbetta M, Snyder AZ, Vincent JL, Raichle ME (2006) Spontaneous neuronal activity distinguishes human dorsal and ventral attention systems. *Proc Natl Acad Sci USA* 103:10046–10051.
3. Golland Y, *et al.* (2007) Extrinsic and intrinsic systems in the posterior cortex of the human brain revealed during natural sensory stimulation. *Cereb Cortex* 17:766–777.
4. Seeley WW, *et al.* (2007) Dissociable intrinsic connectivity networks for salience processing and executive control. *J Neurosci* 27:2349–2356.
5. Beckmann CF, DeLuca M, Devlin JT, Smith SM (2005) Investigations into resting-state connectivity using independent component analysis. *Philos Trans R Soc Lond B Biol Sci* 360:1001–1013.
6. Raichle ME, *et al.* (2001) A default mode of brain function. *Proc Natl Acad Sci USA* 98:676–682.
7. Dosenbach NU, *et al.* (2006) A core system for the implementation of task sets. *Neuron* 50:799–812.
8. Damasio AR (2000) *The Feeling of What Happens*: *Body and Emotion in the Making of Consciousness* (Harcourt, Chicago)
9. Craig AD (2002) How do you feel? interoception: The sense of the physiological condition of the body. *Nat Rev Neurosci* 3:655–666.
10. Critchley HD, Wiens S, Rotshtein P, Ohman A, Dolan RJ (2004) Neural systems supporting interoceptive awareness. *Nat Neurosci* 7:189–195.
11. Naqvi NH, Rudrauf D, Damasio H, Bechara A (2007) Damage to the insula disrupts addiction to cigarette smoking. *Science* 315:531–534.
12. Bunge SA, Ochsner KN, Desmond JE, Glover GH, Gabrieli JD (2001) Prefrontal regions involved in keeping information in and out of mind. *Brain* 124:2074–2086.
13. Crottaz-Herbette S, Anagnoson RT, Menon V (2004) Modality effects in verbal working memory: Differential prefrontal and parietal responses to auditory and visual stimuli. *Neuroimage* 21:340–351.
14. Petrides M (2005) Lateral prefrontal cortex: Architectonic and functional organization. *Philos Trans R Soc Lond B Biol Sci* 360:781–795.
15. Muller NG, Knight RT (2006) The functional neuroanatomy of working memory: Contributions of human brain lesion studies. *Neuroscience* 139:51–58.
16. D'Esposito M (2007) From cognitive to neural models of working memory. *Philos Trans R Soc Lond B Biol Sci* 362:761–772.
17. Koechlin E, Summerfield C (2007) An information theoretical approach to prefrontal executive function. *Trends Cogn Sci* 11:229–235.
18. Miller EK Cohen JD (2001) An integrative theory of prefrontal cortex function. *Annu Rev Neurosci* 24:167–202.
19. Sridharan D, Levitin DJ, Chafe CH, Berger J, Menon V (2007) Neural dynamics of event segmentation in music: Converging evidence for dissociable ventral and dorsal networks. *Neuron* 55:521–532.
20. Menon RS, Luknowsky DC, Gati JS (1998) Mental chronometry using latency-resolved functional MRI. *Proc Natl Acad Sci USA* 95:10902–10907.
21. Formisano E, Goebel R (2003) Tracking cognitive processes with functional MRI mental chronometry. *Curr Opin Neurobiol* 13:174–181.
22. Roebroeck A, Formisano E, Goebel R (2005) Mapping directed influence over the brain using granger causality and fMRI. *Neuroimage* 25:230–242.
23. Crottaz-Herbette S, Menon V (2006) Where and when the anterior cingulate cortex modulates attentional response: Combined fMRI and ERP evidence. *J Cogn Neurosci* 18:766–780.
24. Honey CJ, Kotter R, Breakspear M, Sporns O (2007) Network structure of cerebral cortex shapes functional connectivity on multiple time scales. *Proc Natl Acad Sci USA* 104:10240–10245.
25. Beckmann CF, Smith SM (2004) Probablistic independent component analysis for functional magnetic resonance imaging. *IEEE Trans Med Imaging* 23:137–152.
26. Henson RN, Price CJ, Rugg MD, Turner R, Friston KJ (2002) Detecting latency differences in event-related BOLD responses: Application to words versus nonwords and initial versus repeated face presentations. *Neuroimage* 15:83–97.
27. Sterzer P, Kleinschmidt A (2007) A neural basis for inference in perceptual ambiguity. *Proc Natl Acad Sci USA* 104:323–328.
28. Abler B, *et al.* (2006) Investigating directed influences between activated brain areas in a motor-response task using fMRI. *Magn Reson Imaging* 24:181–185.
31. Efron B, Tibshirani RJ (1993) *An introduction to the bootstrap (Monographs on statistics and applied probability #57*) (CRC Press LLC, Boca Raton, Florida)
30. Mufson EJ, Mesulam MM (1982) Insula of the old world monkey. II: Afferent cortical input and comments on the claustrum. *J Comp Neurol* 212:23–37.
31. Mesulam MM, Mufson EJ (1982) Insula of the old world monkey. III: Efferent cortical output and comments on function. *J Comp Neurol* 212:38–52.
32. Mesulam MM (1998) From sensation to cognition. *Brain* 121(Pt 6):1013–1052.
33. Watson KK, Jones TK, Allman JM (2006) Dendritic architecture of the von economo neurons. *Neuroscience* 141:1107–1112.
34. Allman JM, Watson KK, Tetreault NA, Hakeem AY (2005) Intuition and autism: A possible role for von Economo neurons. *Trends Cogn Sci* 9:367–373.
35. Fan J, McCandliss BD, Fossella J, Flombaum JI, Posner MI (2005) The activation of attentional networks. *Neuroimage* 26:471–479.
36. Posner MI, Rothbart MK (2007) Research on attention networks as a model for the integration of psychological science. *Annu Rev Psychol* 58:1–23.
37. Milham MP, *et al.* (2001) The relative involvement of anterior cingulate and prefrontal cortex in attentional control depends on nature of conflict. *Brain Res Cogn Brain Res* 12:467–473.
38. Baird A, *et al.* (2006) Cognitive functioning after medial frontal lobe damage including the anterior cingulate cortex: A preliminary investigation. *Brain Cogn* 60:166–175.
39. Fellows LK, Farah MJ (2005) Is anterior cingulate cortex necessary for cognitive control? *Brain* 128:788–796.
40. Nee TE, Wagner TD, Jonides J (2007) Interference resolution: Insights from a meta-analysis of neuroimaging tasks. *Cogn Affect Behav Neurosci* 7:1–17.
41. Aron AR, Fletcher PC, Bullmore ET, Sahakian BJ, Robbins TW (2003) Stop-signal inhibition disrupted by damage to right inferior frontal gyrus in humans. *Nat Neurosci* 6:115–116.
42. Robbins TW (2007) Shifting and stopping: Fronto-striatal substrates, neurochemical modulation and clinical implications. *Philos Trans R Soc Lond B Biol Sci* 362:917–932.
43. Aron AR, Robbins TW, Poldrack RA (2004) Inhibition and the right inferior frontal cortex. *Trends Cogn Sci* 8:170–177.
44. Dosenbach NU, *et al.* (2007) Distinct brain networks for adaptive and stable task control in humans. *Proc Natl Acad Sci USA* 104:11073–11078.
45. Hodgson T, *et al.* (2007) The role of the ventrolateral frontal cortex in inhibitory oculomotor control. *Brain* 130:1525–1537.
46. Roberts KL, Hall DA (2008) Examining a supramodal network for conflict processing: A systematic review and novel functional magnetic resonance imaging data for related visual and auditory stroop tasks. *J Cogn Neurosci* 20:1063–1078.
47. Cole MW, Schneider W (2007) The cognitive control network: Integrated cortical regions with dissociable functions. *Neuroimage* 37:343–360.
48. Eichele T, *et al.* (2008) Prediction of human errors by maladaptive changes in event-related brain networks. *Proc Natl Acad Sci USA* 105:6173–6178.
49. Dosenbach NU, Fair DA, Cohen AL, Schlaggar BL, Petersen SE (2008) A dual-networks architecture of top-down control. *Trends Cogn Sci* 12:99–105.
50. Paulus MP (2007) Decision-making dysfunctions in psychiatry–altered homeostatic processing? *Science* 318:602–606.
51. Seeley WW, *et al.* (2008) Frontal paralimbic network atrophy in very mild behavioral variant frontotemporal dementia. *Arch Neurol* 65:249–255.
52. Seth AK (2005) Causal connectivity of evolved neural networks during behavior. *Network Comput Neural Sys* 16:35–54.
53. Dijkstra EW (1959) A note on two problems in connection with graphs. *Numerische Math* 1:269–271.

Supporting Information

Sridharan *et al.* 10.1073/pnas.0800005105

SI Text

Materials and Methods. ***fMRI acquisition.*** Brain images were acquired on a 3T GE Signa scanner using a standard GE whole head coil (software Lx 8.3). For the first (auditory event segmentation) experiment, images were acquired every 2 sec in two runs that lasted 9 min 42 sec and 8 min 48 sec, respectively (for a total of 18 min and 30 sec). The second (visual oddball) and third (resting state) scans were acquired in a single run of 7 min 48 sec and 8 min, respectively. A custom-built head holder was used to prevent head movement. Twenty-eight axial slices (4.0-mm thick, 0.5-mm skip) parallel to the AC-PC line and covering the whole brain were imaged using a T2* weighted gradient echo spiral pulse sequence (TR = 2,000 msec, TE = 30 msec, flip angle = 70 deg, and 1 interleave, in-plane spatial resolution of 3.125 mm) (1). To reduce blurring and signal loss arising from field inhomogeneities, an automated high-order shimming method based on spiral acquisitions was used before acquiring functional MRI scans (2). Images were reconstructed by gridding interpolation and inverse Fourier transform for each time point into $64 \times 64 \times 28$ image matrices (voxel size $3.125 \times 3.125 \times 4.5$ mm). A linear shim correction was applied separately for each slice during reconstruction using a magnetic field map acquired automatically by the pulse sequence at the beginning of the scan (1). fMRI data acquisition was synchronized to stimulus presentation using a TTL pulse sent by EPRIME to the scanner timing board.

fMRI data analysis. fMRI data were preprocessed using SPM2 (http://www.fil.ion.ucl.ac.uk/spm). Functional volumes were corrected for movement-related effects (3), spatially normalized to stereotaxic Talairach coordinates, resampled every 2 mm using sinc interpolation, and smoothed with a 4-mm Gaussian kernel to reduce spatial noise. For the first (auditory segmentation) and second (visual oddball) experiments, statistical analysis was performed using the general linear model (GLM) and the theory of Gaussian random fields as implemented in SPM2. A within-subjects procedure was used to model all of the effects of interest for each subject. Confounding effects of fluctuations in global mean were removed by proportional scaling where, for each time point, each voxel was scaled by the global mean at that time point (4). Low-frequency noise was removed with a high-pass filter (0.5 cycles/min) applied to the fMRI time series at each voxel. Effects of interest for each subject were then defined with the relevant contrasts of the parameter estimates. Group analysis was performed using a random-effects model that incorporated a two-stage hierarchical procedure. In the first stage, contrast images for each subject and each effect of interest were generated as described above. In the second stage, these contrast images were analyzed using a general linear model to determine voxel-wise t statistics. Finally, the t statistics were normalized to Z scores, and significant clusters of activation were determined using the joint expected probability distribution of height and extent of Z scores (5), with height ($Z > 2.33$; $P < 0.01$) and extent thresholds ($P < 0.05$). Maxima and all coordinates are reported in MNI coordinates. Activations were overlaid on a structural Talairach template image using MRIcro (http://www.sph.sc.edu/comd/rorden/mricro.html).

Independent component analysis. Data from the first session of the scan were preprocessed with SPM2 as described above. The preprocessed data were then downsampled to one-half its original resolution (by sampling alternate points) in each dimension to reduce the heavy memory requirements imposed by ICA. ICA was then performed on the preprocessed, downsampled data using the Melodic software package (http://www.fmrib.ox.ac.uk/fsl/). Similar independent components were grouped across subjects using an in-house clustering algorithm; the algorithm computes a similarity metric using the inter-subject correlations of both the spatial map and the associated time course to create groups of similar components across subjects (6). Components in a cluster were then masked with a gray-matter mask and entered into a second random effects analysis (6) and height thresholded at the $P < 0.001$ level, uncorrected, to create group independent component maps.

Calculation of* peak latency *differences. We used the method developed by Henson and colleagues (7) to identify brain regions where the peak of the BOLD response occurred earlier/later relative to the transition. Briefly, this method uses a first-order Taylor approximation (including temporal derivative) in modeling the canonical hemodynamic response function; the ratio of the derivative to canonical parameter estimates provides a measure of the latency differences at each voxel, from which statistical parametric maps may be constructed for each subject. A group map of BOLD latency was then created by entering the individual subject latency images (smoothed with an 8-mm FWHM isotropic Gaussian kernel) into a second-level random-effects analysis. Group-level latency SPMs were masked with voxels that survived the $P < 0.05$ (corrected) level in the F tests in the original SPMs. The group map was height thresholded at $P < 0.025$ uncorrected, and only regions comprising at least ten contiguous voxels are reported.

Calculation of* onset latency *differences. Differences in peak latency of the BOLD response between regions may arise from differences in either the onset or the duration of neural activity (7). Onset latency of the BOLD response provides a means, in principle, of decoupling these possibilities so as to uncover the underlying pattern of neural activity onsets (7–10). We calculated onset latencies according to the method developed by Sterzer and Kleinschmidt (8). This method uses a Fourier model that fits the BOLD response as a linear combination of Fourier basis functions; this removes the need for assuming a response shape *a priori*. The mean time-series extracted from each ROI for each subject was fitted with a sixth-order Fourier basis set (windowed with a Hanning function). Onset latencies were defined as the time at which the slope of the fitted response exceeded 10% of the maximum slope of the ascending part of the response. We then performed a two-sample *t*-test to identify brain regions significantly differing in the onsets of their neural activity ($q < 0.05$, FDR corrected for multiple comparisons).

Granger causality analysis (GCA). GCA was performed in accordance with the methods of Roebroeck *et al.* (11). First, the mean time course from each ROI was extracted for all subjects. This time course was then high-pass filtered at 0.5 cycles per minute. GCA was performed to test for causal influences between ROIs taken pairwise. The order of the autoregressive model used for computation of the influence measure was selected using the Bayesian information criterion. We report the raw values of the directed influence terms for the three tasks in Table S4 *A.1*, *B.1*, and *C.1*. We proceeded to construct a causal connectivity graph (Fig. 3, main text) from these raw F-values as described next.

We performed statistical inference on the causal connections using bootstrap analysis: block-randomized time courses were used to generate an empirical null distribution of influence terms (F-values) and their differences (11) (the difference terms may be obtained by subtracting terms symmetrically situated about the main diagonal in Table S4 *A.1*, *B.1*, and *C.1*). Those directed

connections whose median (across subjects) was significantly different from the median of the null (F-value) distribution (gray arrows in Fig. 3, main text) were identified using a Mann-Whitney *U* test and a stringent threshold ($P < 0.01$, Bonferroni corrected for multiple comparisons). The stringent threshold (and correction) were chosen to avoid potentially spurious causal links introduced by the low temporal resolution and hemodynamic blurring in the fMRI signal. In addition, a difference of influence term ($F_{x\rightarrow y}$ - $F_{y\rightarrow x}$) was used to assess links that showed a dominant direction of influence; the difference term further limits potentially spurious links caused by hemodynamic blurring, and permits the use of a less stringent threshold for group-level testing (11). Again, these dominant links were those wherein the median of the difference of influence term significantly differed from the empirically constructed bootstrap (null) distribution (Mann-Whitney *U* test, $P < 0.05$). Red arrows Fig. 3 (main text) and violet boxes in Table S4 (*A.1*, *B.1*, and *C.1*) highlight these dominant directed connections. P-values for these connections are parenthetically mentioned inside the violet boxes in Table S4 (*A.1*, *B.1*, and *C.1*); furthermore, those *P* values that passed the FDR correction for multiple comparisons are highlighted in blue in the table.

To emphasize the complementarity of the causal and instantaneous connectivity, we also report the instantaneous influence term ($F_{x.y}$) which is an indicator of the classic "zero-lag functional connectivity" between each pair of nodes (11) (Table S4 *A.2*, *B.2*, and *C.2*). A separate analysis confirmed that $F_{x.y}$ is an indicator of the "zero-lag" correlation ("r" value) between pairs of regions: $F_{x.y}$ and "r" values are tightly correlated across pairs of ROIs for all tasks ($r \approx 0.9$, $P < 10^{-4}$). The $F_{x.y}$ and ($F_{x\rightarrow y}$ - $F_{y\rightarrow x}$) terms may be used to infer the relative strength of instantaneous vs. causal(directed) interactions, with the caveat that the instantaneous term is likely artificially inflated due to the temporal smoothing introduced by the hemodynamic response (11). Further, to provide concurrent validity to the GCA approach, we attempted to cluster the six ROIs pairwise to maximize the sum of mutual (pairwise) instantaneous influences ($\Sigma F_{x.y}$). Across all experiments, the most optimal clusters (red boxes in Table S4 *A.2*, *B.2*, and *C.2*) were identical with the SN (rFIC, ACC), CEN (rDLPFC, rPPC), and DMN (VMPFC, PPC), further confirming the functional dissociation between these networks that we observed with ICA.

Granger causality and network analyses with two other task paradigms. GCA was performed in two other datasets: (a) A visual "oddball" attention task (12) employing 13 participants, and (b) a resting state scan employing 22 participants. These data were chosen because they involve entirely different stimulus modalities and task requirements. The visual oddball task showed right-lateralized activation of the SN and CEN regions and deactivation of the DMN regions during the perception of the infrequent (as contrasted with frequent) stimuli (data not shown). Similarly, statistical parametric latency maps, as computed by the method of Henson *et al.* (7) revealed that the rFIC and ACC had earlier peak latency compared to other regions in the CEN and DMN (data not shown).

For the visual oddball task, ROIs were defined at each key (SN/CEN/DMN) network region as spheres centered at the peaks of activation (or deactivation) and with radii raging from 6–10 mm. ROIs for the resting state task were the same as those used for the auditory event segmentation task. Time courses were extracted from each ROI, and bivariate GCA was performed as described above for each ROI pair for each task. Network statistics were computed on these causal networks in a manner similar to that described in the main text (see *Materials and Methods*).

Discussion. ***Potential confound: neural vs. vascular effects.*** Information flow between networks of neurons occurs over the timescale of several tens to hundreds of milliseconds, whereas with fMRI we are constrained to imaging the slow variations in the BOLD signal that occurs on the order of a few seconds (albeit with excellent spatial resolution that is impossible to achieve with other scalp-recording techniques that have better temporal resolution, such as electro-encephalograpy or magneto-encephalography). Hence, one potential caveat while performing chronometric and causal analyses on the BOLD signal is that the observed effects may reflect vascular rather than neural dynamics. However, we present several lines of evidence that argue against this possibility:

(*i*) Previous studies have used chronometric techniques, such as onset latency analysis, with carefully controlled experimental designs, to show that the relative timing between onsets of the BOLD responses between different regions can be used as a predictor of differences in neural activity onset, and can resolve these differences with a temporal accuracy of tens to hundreds of milliseconds (8–10)

(*ii*) In a previous analysis of a Sternberg working memory task, wherein a visual stimulus precedes motor response, we have shown, using onset latency chronometric analysis, that the BOLD signal onsets earlier in sensory (visual), compared to motor areas. Similarly, GCA detected a causal influence from the visual to motor areas (13), as expected.

(*iii*) Two recent studies have shown that the BOLD signal is tightly coupled with gamma (30–70 Hz) band-limited-power (BLP) of the intracranial EEG in the visual and auditory cortices (14, 15). Several previous studies have shown that there is increased gamma band activity during visual or tactile attention in primates and humans (16, 17), and during human conscious perception [intracranial EEG recordings, (18)]. Hence, it is plausible that the BOLD signal fluctuations in the CEN and DMN that appear to be caused by the rFIC (Fig. 3, main text) reflect attentional control mechanisms, mediated by gamma power coupling between these regions, that underlie the CEN-DMN switch.

(*iv*) Consistent latency differences and causal effects were observed across three different datasets, each with a large number of subjects, using random effects analyses.

(*v*) The brain regions probed in our study are served by multiple cerebral arteries, so the timing of vascular changes are unlikely to be coupled in any significant way. Moreover, it is plausible to assume that the distribution of vasculature is roughly symmetric across hemispheres: in this case, one would expect that the vascular dynamics in the right hemispheric regions to be mirrored (or closely approximated) by their left hemispheric counterparts. However, in our analysis this was not the case: latency and causal connectivity analysis on the corresponding left hemispheric regions indicated a less robust, and more variable effects, the dynamics were not similar to those of their right hemispheric counterparts (across tasks and subjects); left hemispheric regions often failed to show statistically significant causal and latency effects (Fig. S3).

These lines of evidence increase confidence, and further confirm, that our findings directly reflect the underlying neural processes.

Choice of regions of interest. In the causal connectivity and network analyses outlined in the main text, we have confined ourselves to the six key nodes of the SN, CEN, and DMN, and specifically to the right hemisphere. Since our question of interest was the mechanism of switching between the CEN and DMN, only those regions that showed significant latency differences with the CEN and DMN regions (as assessed by the whole brain peak latency analysis, Fig. S1 and Table S2) were selected for further analysis. In our analysis, only the SN nodes (FIC and ACC) in the prefrontal cortex showed peak latency differences consistently across both auditory segmentation and visual oddball tasks. Hence, we included only the FIC and the ACC (along with the

nodes of the CEN and DMN) for subsequent GCA and network analyses. In this section we briefly discuss control analyses performed with brain regions that could play a role in the switching process, including the left hemispheric counterparts of the FIC, DLPFC, and PPC, the temporoparietal junction (TPJ), a key node implicated in directing bottom-up attention to salient environmental stimuli (19, 20) as well as sensory regions (primary auditory and visual cortex) that could trigger bottom-up signaling

(i) Left hemispheric regions in the SN, CEN, and DMN. Our previous GLM analysis of the auditory event segmentation task data revealed that level of activity in the left hemispheric regions (FIC, DLPFC, and PPC) was significantly lower than that of the corresponding right hemispheric regions [figure 4 in (13)]. GLM analysis of the visual oddball task also indicated significant right lateralization of responses in the regions of interest (12). Hence, we hypothesized that the signals in the left hemispheric regions might be less robust and other effects such as latency, and causality would be correspondingly weaker. There was evidence of this in an analysis of the auditory segmentation task: while the mean onset latencies of the right and left FICs did not differ significantly (two sample t-test, $P > 0.05$), the left FIC onset latencies were highly variable across subjects (0.61 ± 0.62 s, mean $\pm$ SD), compared with the right FIC (0.40 ± 0.18 s). This led to far fewer regions showing significant onset latency differences with the left FIC (only PCC, data not shown), as compared with the right FIC that showed significant latency differences with almost all of the CEN and DMN regions (Fig. 2 in main text). Similarly, the left PPC did not show significant onset latency differences with any region.

To perform connectivity and network analyses on the left hemispheric regions, we defined the following ROIs in the left hemisphere: left-hemispheric FIC (lFIC) and left-hemispheric PPC (lPPC) ROIs were defined as spheres of 6–10-mm radius centered around the peaks of the ICA activation clusters (Table S1); the left-hemispheric DLPFC (lDLPFC) ROI was derived from its right-hemispheric counterpart (Table S1) by reflection about the x = 0 mm sagittal plane. The ACC, VMPFC, and PCC ROIs were identical to ones used in the analysis reported in the main text. Time courses were extracted using Marsbar, and connectivity (GCA) and network analysis were performed as described in the Materials and Methods section in the main text. This analysis revealed that the left FIC did not differ significantly from any of the other regions in its causal outflow (out-in degree) (Fig. S3*A*), or path length (data not shown). Repeating this analysis with the visual oddball and task-free resting state data revealed that the net causal outflow of the left FIC differed from very few regions (Fig. S3 *B* and *C*), whereas the right FIC had a much more robust difference in net causal outflow across all three tasks (compare with Fig. 4, main text).

(ii) Sensory regions vis-à-vis the SN, CEN and DMN. In the present study, the auditory segmentation and visual oddball tasks used different sensory modalities, whereas the resting state task did not require any explicit (task-based) sensory information processing. In fact, analysis of the resting state data also showed that the FIC can exert causal influences across networks without any explicit stimulus. Hence, in the analysis reported in the main text, sensory regions were excluded from connectivity and network analysis to emphasize commonality of directional information flow, and the critical role of the FIC across tasks.

However, examination of the influences of sensory signals on the three networks remains an important open problem. Does the rFIC merely relay bottom-up sensory information from the sensory regions to the other nodes, or truly exert top-down control on the other nodes? To address this question, we performed onset latency and GCA on ROIs in the sensory cortices vis-à-vis the three networks. Briefly, we defined regions of interest as spheres of 6–8-mm radius in the bilateral auditory cortex (Heschl's gyrus, for the auditory segmentation task, MNI coordinates: [$\pm$53, $-$8, 4]mm) and bilateral visual cortex (lingual gyrus, Brodmann Area 18, for the visual oddball task, MNI coordinates: [$\pm$9, $-$82, $-$7]mm). We extracted the time series from these regions as before (see Materials and Methods). It must be noted that, in Experiment 1 (auditory event segmentation), activation in the auditory cortex was positively correlated with amplitude changes in the music; we did not detect any region in the auditory cortex that increased its activity in response to decreased sound amplitude (13). Thus, at the events of interest (musical movement transitions), which are accompanied by a brief silence, we expected auditory cortex activity to be diminished (and this was indeed what we found using a GLM analysis, data not shown). Hence, the time series of the auditory cortices were inverted before further analysis (similar to the VMPFC and PCC, as in Fig. S2), because we hypothesized that the onset of the decrease in activity could, in fact, provide a signal to higher areas and/or prefrontal regions. For Experiment 2 (visual oddball), no such inversion of the signals from the visual cortex was considered necessary.

Latency analysis of the signals from the sensory cortices revealed that the onset latency of these regions did not differ significantly from the rFIC (two-sample t test, $P > 0.05$, Bonferroni correction for multiple comparisons). The auditory and visual cortices demonstrated early onsets (median of 0.3 s to 0.4 s; comparable to the rFIC) although these differences were not statistically significantly different from the other regions (two-sample t test, $P > 0.05$). Similarly, GCA on a network including the sensory regions for the auditory segmentation task revealed a mean $F_{x\to y}$ of 0.0365 from auditory cortex to the rFIC and 0.0323 from the rFIC to the auditory cortex ($P < 0.01$, Mann-Whitney U test, Bonferroni correction for multiple comparisons): the dominant direction of influence (difference term, $F_{x\to y} - F_{y\to x}$) was from the auditory cortex to the rFIC, but this did not reach significance ($P > 0.05$, Mann-Whitney U test). On the other hand, this trend was reversed in the visual oddball task, with a mean $F_{x\to y}$ of 0.0286 from visual cortex to rFIC and 0.0465 from rFIC to visual cortex; again, the dominant direction of influence (in this case from rFIC to visual cortex) did not reach significance. Overall, we found that while there was some evidence of early onset in the sensory cortices across tasks, the directionality of information flow (to and from the rFIC) could not be unambiguously resolved. One possibility here is that there is some sort of early but weak signaling from the sensory regions that is amplified by the FIC. Again, the lack of robust latency differences between the sensory regions and the FIC may be due to the relative insensitivity of fMRI to detect small latency differences. Hence, a proper examination of this issue may require simultaneous EEG and fMRI recordings (12).

(iii) The role of the right temporo-parietal junction (rTPJ) vis-à-vis the right fronto-insular cortex (rFIC) in attention switching. Corbetta & Shulman (19) proposed that the rTPJ is an important component of the bottom-up salience detection system (redirecting endogenous attention to external stimuli). Our data suggest that the rFIC may have primacy in initiating the control signals responsible for switching between endogenous (default-mode) and exogenous attentional systems. In a more recent study, Shulman *et al.* (20) investigated several coordinates in the TPJ region. Of special relevance are two subregions in the right TPJ (rTPJ): one more dorsal (Talairach coordinates: 45, $-$49, 46; or MNI coordinates: 46, $-$52, 47), and the second more ventral (Talairach coordinates: 52, $-$49, 26; or MNI coordinates 53, $-$52, 26). The former region lies in close proximity to the rPPC region that was the focus of our study (MNI coordinates: 54, $-$50, 50). Our analysis indicates that the rFIC had a consistently earlier peak and onset latency compared to the rPPC (Fig. 2, Fig. S1); connectivity and network analyses also demonstrate that the rFIC also has a significantly higher net causal outflow than the rPPC (see Fig. 4,

main text). Intriguingly, the rPPC appeared to relay information from the rFIC to the DMN regions (PCC and VMPFC) in the visual oddball and resting state tasks (Fig. 3 *B* and *C*, main text) indicating that the rPPC may mediate deactivation of the DMN regions based on a control signal from the rFIC.

The latter (more ventral) rTPJ subregion is more proximal to the classic TPJ implicated in detecting changes in the sensory environment (19, 21). We performed control analyses on this region (identified on the basis of GLM activation clusters) for both the auditory segmentation (8-mm sphere centered at [54, −44, 20]mm, MNI) and visual oddball (8-mm sphere centered at [57, −46, 18]mm, MNI) task. These analyses indicated that the rTPJ has an onset that followed the rFIC (mean onset difference 0.25 s for auditory segmentation task, and 0.8 s for the visual oddball task, rFIC leading), but these differences were not statistically significant (two-sample *t*-test, $P > 0.05$). GCA and subsequent network analyses indicated that the dominant causal influence direction in the auditory segmentation task was from the rFIC to the rTPJ with a mean $F_{x\to y}$ of 0.0350 from rFIC to the rTPJ (F:rFIC→rTPJ) and 0.0219 in the reverse direction (F:rTPJ→rFIC) ($P < 0.01$, Mann-Whitney *U* test, Bonferroni correction for multiple comparisons); however, the dominant direction of influence (difference term, $F_{x\to y} - F_{y\to x}$) did not reach significance ($P < 0.05$, Mann-Whitney *U* test). For the visual oddball task these numbers were 0.0620 (F:rFIC→rTPJ) and 0.0474 (F:rTPJ→rFIC), respectively ($P < 0.01$, Mann-Whitney *U* test, Bonferroni correction for multiple comparisons). Moreover, the dominant direction of influence from rFIC to rTPJ was significant at the $P < 0.05$ level (Mann-Whitney *U* test) (Fig. S4). The rFIC also appeared to be more of a central network hub with a higher net causal outflow (1.9 and 1.8 for the two tasks) compared with the rTPJ (0.6 and 0.3 for the two tasks), and shorter path length (1.20 and 1.56 vs. 1.35 and 1.59) although these differences were not statistically significant (two-sample *t*-test, $P > 0.05$) after correcting for multiple comparisons.

In summary, our findings indicate that the rFIC in fact precedes and exerts causal influences on the rTPJ, rather than the other way round, and leads us to hypothesize that the rFIC may, in fact, be the primal circuit breaker that helps redirect endogenous attention in response to salient environmental stimuli.

A brief discussion on Granger Causality Analysis. ***(i) Latency (fMRI mental chronometry) and Granger causality analyses.*** We have used several analyses techniques, viz., peak, onset, and Granger Causality analyses, to examine the dynamics of response in the six key regions of the SN, CEN, and DMN. Here we provide a brief description of how these analyses relate to, and complement each other. The peak latency analysis of (7), provides a statistical parametric map of peak BOLD latencies across the entire brain, which can be used as a starting point for identifying key regions wherein the BOLD response peaks earlier or later, which may be taken as a basic indicator of the relative latency of the underlying neural responses. However, a precise quantification of the latencies in these regions using this approach is not possible due to high estimation errors in the derivative to canonical ratio (7). Moreover, responses of different amplitudes that onset at the same times may peak at different times (with the larger amplitude response having a later peak). To overcome these limitations, we performed onset latency analysis on key regions in the SN, CEN, and DMN [according to the method of Sterzer and Kleinschmidt (8)], which provides a better measure of the relative underlying neural latency differences. Thus, these analyses are complementary, and while one expects early onset regions to also have early peaks (such as we observe in the rFIC), in theory the results from the two analyses need not necessarily overlap.

Again, while peak and onset latency analyses can demonstrate precedence of activation between the CEN-DMN nodes and rFIC, these cannot directly address the presence (or absence) of top-down control that the rFIC would exert on the CEN and DMN regions (22). On the other hand, GCA provides a more principled way to assess top-down control across task paradigms, since it involves contributions from both the stimulus locked BOLD signal as well as stochastic components that are not necessarily stimulus locked (11). In this sense, the two types of analyses are complementary. Findings from onset latency resolved chronometry (fMRI mental chronometry) and GCA need not necessarily overlap, although in practice we do observe significant overlap between these. For instance, the earlier peak and onset latencies of the FIC in the SN are reflective of the underlying causal connectivity pattern with maximal outflow from the FIC across tasks. However, earlier onset alone does not necessarily correspond to a high causal outflow, as evidenced in the ACC, which has a relatively low, and sometimes even negative net causal outflow. These findings are in line with previous observations on these analyses (10, 11, 13, 22).

(ii) Relationship between zero-lag functional connectivity, independent component and Granger causality (causal connectivity) analyses. In our analysis, we have used ICA to show the statistical independence between the SN, CEN, and DMN. ICA performs spatial decomposition to generate maximally independent spatial maps each with an associated timecourse. Each voxel in a spatial ICA map has an identical time-course (except for a scale factor) (23). In this sense, ICA is analogous to functional connectivity in that it identifies spatial clusters of voxels in the brain that have high zero-lag correlations. Moreover, ICA goes beyond traditional functional connectivity analyses by ensuring that noise related components (related to movement, etc.) are factored out of the voxels before the zero-lag spatial correlation maps are computed. There is a fundamental difference between "functional connectivity" as assessed by zero-lag correlation analysis (such as ICA) and "causal connectivity" as assessed by GCA. While ICA decouples these regions (shows them to be functionally disconnected) based on instantaneous correlations, GCA attempts to capture the power of a region's signal to predict the future signal in another region, and evaluates whether these regions are functionally coupled based on the history of the signals (24). For instance, while there is no instantaneous correlation between the different networks, it is possible that these regions are correlated in a time-shifted fashion. While previous studies have shown that the signal in the DMN and CEN/SN are anti-correlated (25, 26), our study replicates this result, and further shows that the BOLD signal in the SN has a shorter onset latency compared to the CEN and the DMN (Fig. 2 and Fig. S2 in our study). GCA exploits this temporal precedence information in a statistical (biviriate/multivariate autoregressive) framework to compute "causal" connectivity between brain regions. However, as a special case, GCA can also be used to capture zero lag correlations using the "instantaneous" term $F_{x.y}$, which approximately corresponds to the residual interactions remaining that could not be assigned a specific directionality (11). Indeed, we found that pairwise clustering of regions based on the instantaneous F term (described previously), revealed that across all experiments, the most optimal clusters (red boxes in Table S4 *A.2*, *B.2*, and *C.2*) were identical with the SN (rFIC, ACC), CEN (rDLPFC, rPPC), and DMN (VMPFC, PPC). Thus, we were able to provide concurrent validity to the GCA approach by confirming the functional dissociation between these networks that we had already observed with ICA (Fig. 1, main text).

1. Glover GH, Lai S (1998) Self-navigated spiral fMRI: Interleaved versus single-shot. *Magn Reson Med* 39:361–368.
2. Kim DH, Adalsteinsson E, Glover GH, Spielman DM (2002) Regularized higher-order in vivo shimming. *Magn Reson Med* 48:715–722.
3. Friston KJ, Williams S, Howard R, Frackowiak RS, Turner R (1996) Movement-related effects in fMRI time-series. *Magn Reson Med* 35:346–355.
4. Macey PM, Macey KE, Kumar R, Harper RM (2004) A method for removal of global effects from fMRI time series. *Neuroimage* 22:360–366.
5. Poline JB, Worsley KJ, Evans AC, Friston KJ (1997) Combining spatial extent and peak intensity to test for activations in functional imaging. *Neuroimage* 5:83–96.
6. Esposito F, *et al.* (2005) Independent component analysis of fMRI group studies by self-organizing clustering. *Neuroimage* 25:193–205.
7. Henson RN, Price CJ, Rugg MD, Turner R, Friston KJ (2002) Detecting latency differences in event-related BOLD responses: Application to words versus nonwords and initial versus repeated face presentations. *Neuroimage* 15:83–97.
8. Sterzer P, Kleinschmidt A (2007) A neural basis for inference in perceptual ambiguity. *Proc Natl Acad Sci USA* 104:323–328.
9. Formisano E, Goebel R (2003) Tracking cognitive processes with functional MRI mental chronometry. *Curr Opin Neurobiol* 13:174–181.
10. Menon RS, Luknowsky DC, Gati JS (1998) Mental chronometry using latency-resolved functional MRI. *Proc Natl Acad Sci USA* 95:10902–10907.
11. Roebroeck A, Formisano E, Goebel R (2005) Mapping directed influence over the brain using granger causality and fMRI. *Neuroimage* 25:230–242.
12. Crottaz-Herbette S, Menon V (2006) Where and when the anterior cingulate cortex modulates attentional response: Combined fMRI and ERP evidence. *J Cogn Neurosci* 18:766–780.
13. Sridharan D, Levitin DJ, Chafe CH, Berger J, Menon V (2007) Neural dynamics of event segmentation in music: Converging evidence for dissociable ventral and dorsal networks. *Neuron* 55:521–532.
14. Privman E, *et al.* (2007) Enhanced category tuning revealed by intracranial electroencephalograms in high-order human visual areas. *J Neurosci* 27:6234–6242.
15. Nir Y, *et al.* (2007) Coupling between neuronal firing rate, gamma LFP, and BOLD fMRI is related to interneuronal correlations. *Curr Biol* 17:1275–1285.
16. Womelsdorf T, Fries P, Mitra PP, Desimone R (2006) Gamma-band synchronization in visual cortex predicts speed of change detection. *Nature* 439:733–736.
17. Bauer M, Oostenveld R, Peeters M, Fries P (2006) Tactile spatial attention enhances gamma-band activity in somatosensory cortex and reduces low-frequency activity in parieto-occipital areas. *J Neurosci* 26:490–501.
18. Meador KJ, Ray PG, Echauz JR, Loring DW, Vachtsevanos GJ (2002) Gamma coherence and conscious perception. *Neurology* 59:847–854.
19. Corbetta M, Shulman GL (2002) Control of goal-directed and stimulus-driven attention in the brain. *Nat Rev Neurosci* 3:201–215.
20. Shulman GL, Astafiev SV, McAvoy MP, d'Avossa G, Corbetta M (2007) Right TPJ deactivation during visual search: Functional significance and support for a filter hypothesis. *Cereb Cortex* 17:2625–2633.
21. Downar J, Crawley AP, Mikulis DJ, Davis KD (2000) A multimodal cortical network for the detection of changes in the sensory environment. *Nat Neurosci* 3:277–283.
22. Goebel R, Roebroeck A, Kim DS, Formisano E (2003) Investigating directed cortical interactions in time-resolved fMRI data using vector autoregressive modeling and granger causality mapping. *Magn Reson Imaging* 21:1251–1261.
23. Beckmann CF, Smith SM (2004) Probabilistic independent component analysis for functional magnetic resonance imaging. *IEEE Trans Med Imaging* 23:137–152.
24. Miller BT, D'Esposito M (2005) Searching for ''the top'' in top-down control. *Neuron* 48:535–538.
25. Greicius MD, Krasnow B, Reiss AL, Menon V (2003) Functional connectivity in the resting brain: A network analysis of the default mode hypothesis. *Proc Natl Acad Sci USA* 100:253–258.
26. Fox MD, Snyder AZ, Zacks JM, Raichle ME (2006) Coherent spontaneous activity accounts for trial-to-trial variability in human evoked brain responses. *Nat Neurosci* 9:23–25.

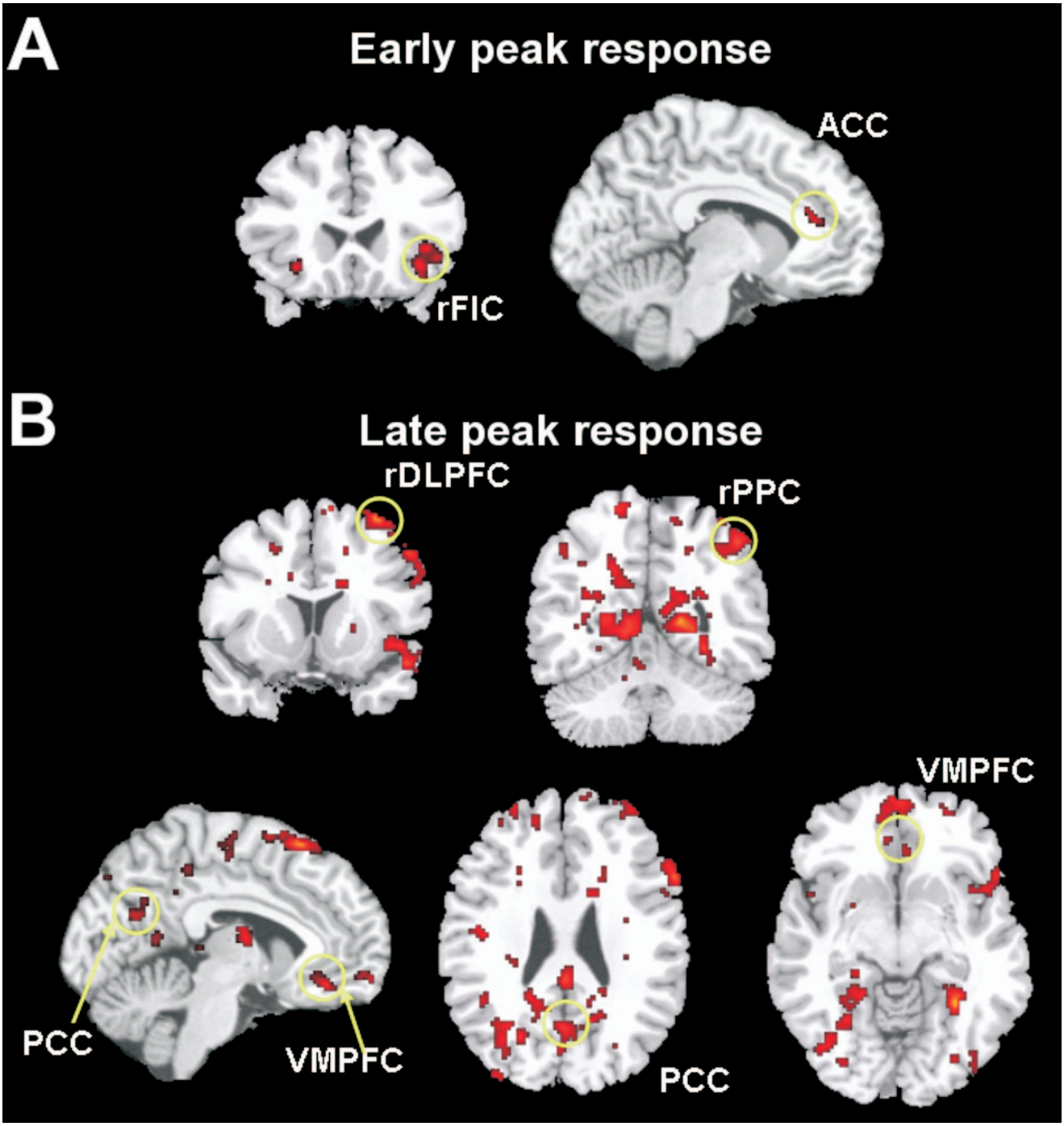

Fig. S1. Differential response latencies at the transition during auditory event segmentation. Latency analysis at the transition revealed early activation in the FIC and ACC, and late activation in the nodes of the CEN and DMN (rDLPFC, rPPC, PCC, and VMPFC). All slices are identical with the slices shown in Fig. 1 of main text, in addition panel (*A*) highlights early response in the ACC in a sagittal slice (see also accompanying Table S2).

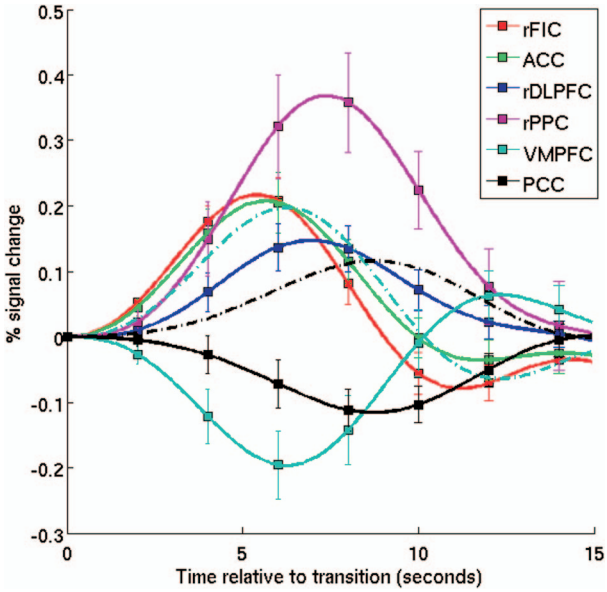

Fig. S2. BOLD response fitted by a Fourier model in the key network regions during auditory event segmentation. The BOLD response was fitted by a sixth-order Fourier model in each of the key nodes of the networks. The fitted responses were averaged across events and subjects for each node and plotted as a percentage signal change from baseline following the occurrence of the event (transition) at t = 0 s. It can be seen that peak activation in the FIC and ACC precedes both peak deactivation in the VMPFC and PCC, and peak activation in the rDLPFC and rPPC. For clarity, the inverted responses in the VMPFC and PCC are shown as dot-dashed lines. Error bars at each TR (2 s) show S.E.M. of the fitted responses across subjects. These fitted responses were further used to define the onset latency for each region (Fig. 2 in main text).

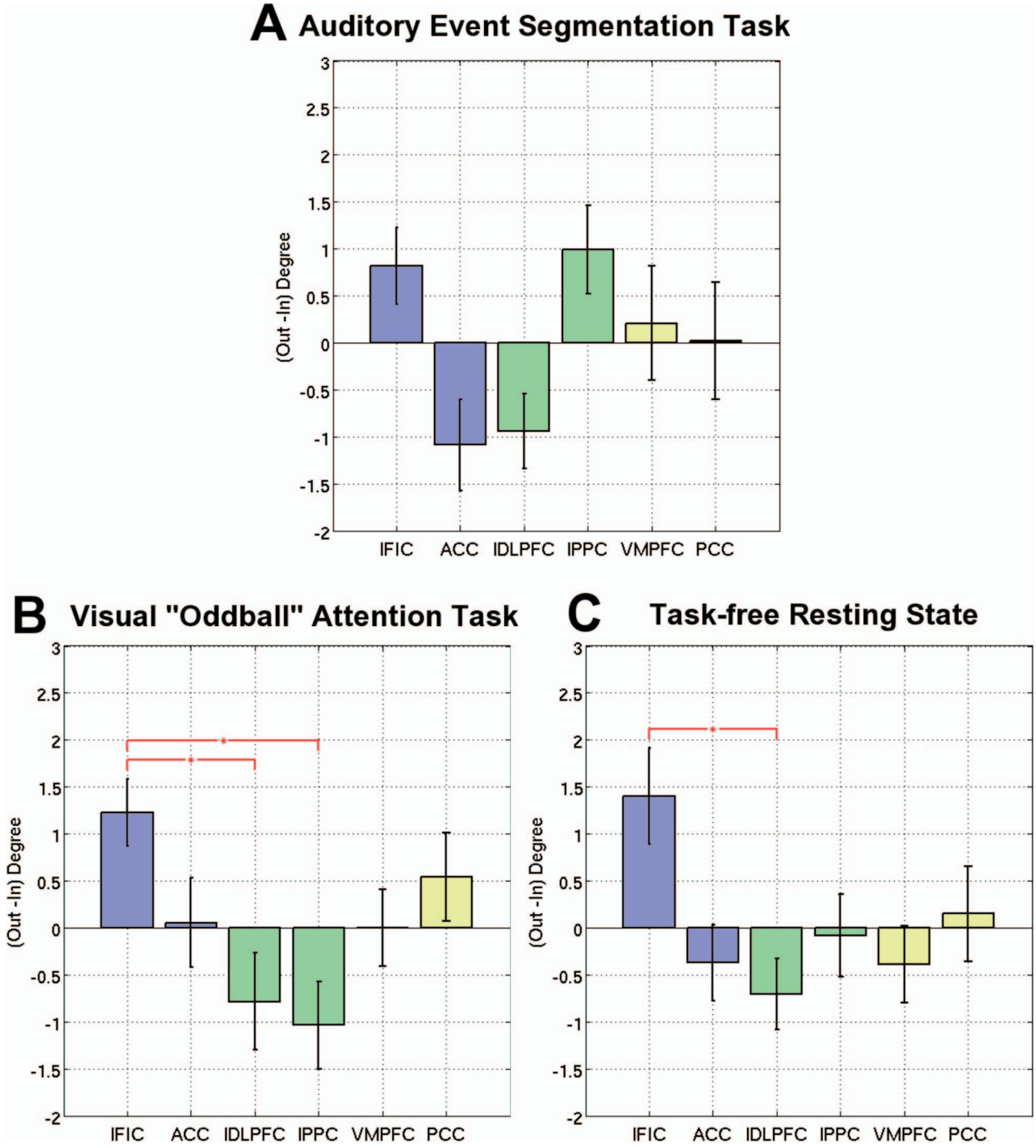

Fig. S3. Net causal outflow (out-in degree) of the left-hemispheric nodes of the Salience, Central-Executive, and Default-Mode Networks in the three experiments. Comparison of the net causal outflow (out-in degree) for the left-hemispheric nodes of the Salience, Central-Executive, and Default-Mode networks (conventions as in Fig. 2, main text). The net causal outflow of the left FIC did not differ significantly from other regions in its causal ''out-in'' degree (a measure of net causal outflow) in a consistent manner across tasks (two-sample test, $q > 0.05$, FDR correction for multiple comparisons), whereas the right FIC had a much more robust difference in net causal outflow across all three tasks (compare with Fig. 4, main text).

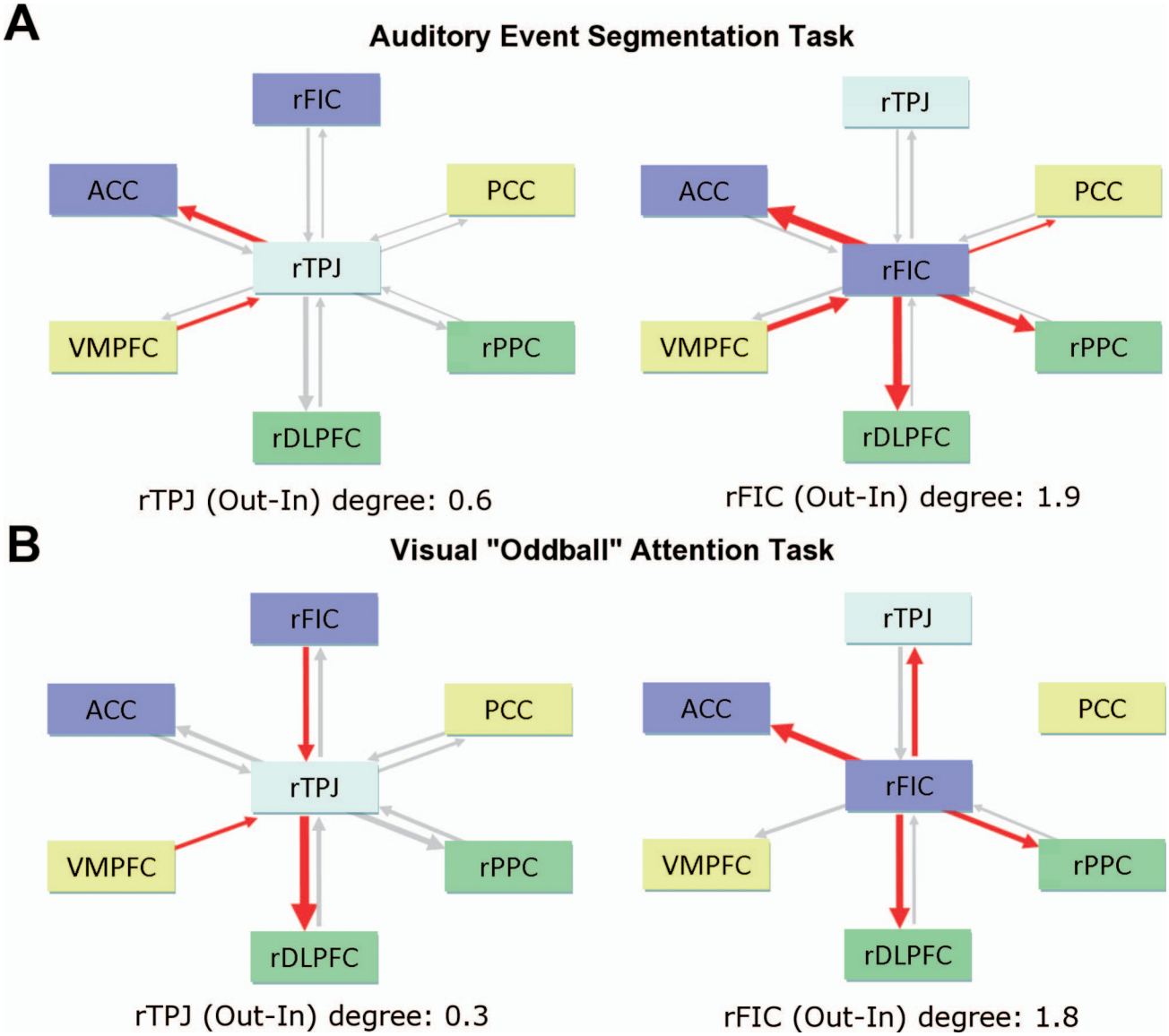

Fig. S4. Granger causality analysis network diagram of the rTPJ and rFIC for the auditory segmentation and visual oddball tasks. Bivariate GCA on the rTPJ (left panel) and rFIC (right panel) with the key nodes of the CEN and DMN in the auditory event segmentation (*A*) and visual oddball (*B*) tasks revealed that the dominant direction of influence was from the rFIC to the rTPJ for both tasks (conventions as in Fig. 3, main text). The rFIC also had a consistently higher net causal outflow (out-in degree, indicated at the bottom of each panel) across both tasks, suggesting that the rFIC may have overall primacy in initiating the switch between exogenous and endogenous attentional systems in the brain [the apparent discrepancy between the net causal outflow values of the rFIC reported here and Fig. 4 (main text), and Table S5, arises from the rTPJ being included here as an additional node in the network analysis].

Table S1. Coordinates of SN, CEN, and DMN regions from ICA-derived clusters of the auditory event segmentation task

Regions	R/L	BA	Peak-MNI cords, mm	Z-Score
Fronto-insular Cortex (FIC)	R	47	37 25 −4	4.98
	L	47	−32 24 −6	4.58
Anterior Cingulate Cortex (ACC)	R/L	24/32	4 30 30	5.80
Dorsolateral Prefrontal Cortex (DLPFC)	R	9	45 16 45	5.14
Posterior Parietal Cortex (PPC)	R	40	54 −50 50	6.18
	L	40	−38 −53 45	4.90
Ventromedial Prefrontal Cortex (VMPFC)	R/L	11	−2 36 −10	4.92
Posterior Cingulate Cortex (PCC)	R/L	23/30	−7–43 33	6.36

Abbreviations: BA, brodmann area; R/L, right or left.

Table S2. Coordinates of SN, CEN, and DMN cluster peaks from peak latency analysis of the auditory event segmentation task (refer to Figure S1)

Regions	R/L	BA	Peak-MNI cords (mm)
Fronto-insular Cortex (FIC)	R	47	34 26 −6
	L	47	−32 25 −10
Anterior Cingulate Cortex (ACC)	R/L	24/32	7 33 19
Dorsolateral Prefrontal Cortex (DLPFC)	R	9	50 15 43
Posterior Parietal Cortex (PPC)	R	40	50 −50 51
	L	40	−46 −50 44
Ventromedial Prefrontal Cortex (VMPFC)	R/L	11	3 37 −14
Posterior Cingulate Cortex (PCC)	R/L	23/30	1 −60 30

Abbreviations: BA, brodmann area; R/L, right or left.

Table S3. Onset latency differences between ROIs during auditory event-segmentation

ROI	rFIC	ACC	rDLPFC	rPPC	VMPFC	PCC
rFIC	N.A.	**0.4958** (*t*=-1.1215, *P*= 0.1163)	**2.0882** (*t*=-3.5800, *P*= 0.0076)	**1.4160** (*t*=-2.3202, *P*= 0.0032)	**1.1345** (*t*=-1.8567, *P*= 0.0031)	**1.7941** (*t*=-2.8595, *P*= 0.0017)
ACC	x	N.A	**1.5924** (*t*=-3.2054, *P*= 0.0528)	**0.9202** (*t*=-2.0128, *P*= 0.0959)	**0.6387** (*t*=-1.5862, *P*= 0.1793)	**1.2983** (*t*=-2.5277, *P*= 0.0391)
rDLPFC	x	x	N.A	**-0.6723** (*t*=-1.0678, *P*= 0.4371)	**-0.9538** (*t*=-0.6990, *P*= 0.2485)	**-0.2941** (*t*=-1.5349, *P*= 0.7454)
rPPC	x	x	x	N.A	**-0.2815** (*t*=-0.8692, *P*= 0.6217)	**0.3782** (*t*=-1.7701, *P*= 0.5839)
VMPFC	x	x	x	x	N.A	**0.6597** (*t*=-1.9409, *P*= 0.3021)
PCC	x	x	x	x	x	N.A

Onset latency differences in seconds (row ROI relative to column ROI). Positive latency differences indicate "row" ROI onsets after "column" ROI (vice versa for negative differences). Significant onset latency differences are highlighted in violet boxes ($P < 0.01$, two-sample *t* test). All highlighted regions also showed significant onset latency differences after FDR correction for multiple comparisons ($q < 0.05$, highlighted in blue, see also Figure 2).

Table S4. Mean GCA directed influence and instantaneous influence F values between pairs of regions for the three experiments

(A) Auditory event segmentation task

(A.1) Directed influence F values (mean ± SE across subjects)

F(x→y)	rFIC	ACC	rDLPFC	rPPC	VMPFC	PCC
rFIC	-	0.031±0.007	0.025±0.007	0.021±0.007	0.064±0.015 (0.0056)	0.028±0.008
ACC	0.092±0.020 (0.0000)	-	0.036±0.009	0.023±0.006	0.037±0.009	0.032±0.006
rDLPFC	0.088±0.021 (0.0000)	0.030±0.008	-	0.032±0.007	0.031±0.010	0.034±0.007 (0.0414)
rPPC	0.069±0.015 (0.0005)	0.033±0.007	0.029±0.007	-	0.032±0.008	0.015±0.004
VMPFC	0.033±0.006	0.036±0.007	0.030±0.006	0.022±0.004	-	0.029±0.008
PCC	0.029±0.004 (0.0029)	0.027±0.006	0.024±0.005	0.023±0.007	0.037±0.006	-

(A.2) Instantaneous influence F values (mean ± SE across subjects)

F(x.y)	rFIC	ACC	rDLPFC	rPPC	VMPFC	PCC
rFIC	-	0.354±0.047	0.125±0.031	0.121±0.028	0.126±0.029	0.132±0.037
ACC	x	-	0.298±0.064	0.193±0.044	0.072±0.016	0.207±0.049
rDLPFC	x	x	-	0.317±0.055	0.039±0.012	0.242±0.047
rPPC	x	x	x	-	0.027±0.009	0.144±0.032
VMPFC	x	x	x	x	-	0.107±0.021
PCC	x	x	x	x	x	

Table S4. (*Continued*).

(B) Visual oddball attention task

(B.1) Directed influence F values (mean ± SE across subjects)

F(x→y)	rFIC	ACC	rDLPFC	rPPC	VMPFC	PCC
rFIC	-	0.036±0.010	0.036±0.011	0.034±0.005	0.065±0.021	0.042±0.022
ACC	0.078±0.011 (0.0010)	-	0.022±0.004	0.028±0.009	0.035±0.008	0.033±0.007
rDLPFC	0.076±0.015 (0.0044)	0.045±0.014	-	0.049±0.012 (0.0303)	0.028±0.005	0.043±0.024
rPPC	0.058±0.015 (0.0286)	0.036±0.007 (0.0500)	0.024±0.005	-	0.039±0.009	0.022±0.006
VMPFC	0.042±0.009	0.034±0.010	0.034±0.011	0.036±0.010	-	0.051±0.021
PCC	0.033±0.010	0.030±0.009	0.023±0.005	0.032±0.006 (0.0052)	0.030±0.006	-

(B.2) Instantaneous influence F values (mean ± SE across subjects)

F(x.y)	rFIC	ACC	rDLPFC	rPPC	VMPFC	PCC
rFIC	-	0.420±0.069	0.176±0.027	0.232±0.037	0.101±0.065	0.126±0.038
ACC	x	-	0.241±0.053	0.264±0.052	0.057±0.020	0.211±0.047
rDLPFC	x	x	-	0.462±0.047	0.041±0.020	0.084±0.033
rPPC	x	x	x	-	0.050±0.014	0.156±0.057
VMPFC	x	x	x	x	-	0.082±0.022
PCC	x	x	x	x	x	-

Table S4. (*Continued*).

(C) Task-free resting state

(C.1) Directed influence F values (mean ± SE across subjects)

F(x→y)	rFIC	ACC	rDLPFC	rPPC	VMPFC	PCC
rFIC	-	0.049±0.008	0.036±0.008	0.031±0.005	0.044±0.008	0.042±0.009
ACC	0.110±0.014 (0.0000)	-	0.036±0.006	0.028±0.004	0.05±50.011	0.047±0.008
rDLPFC	0.069±0.007 (0.0000)	0.041±0.007	-	0.042±0.006	0.031±0.006	0.059±0.013
rPPC	0.063±0.009 (0.0001)	0.038±0.007	0.040±0.009	-	0.024±0.006	0.041±0.008
VMPFC	0.044±0.008	0.065±0.012	0.036±0.006	0.033±0.006 (0.0426)	-	0.065±0.013
PCC	0.079±0.013 (0.0013)	0.048±0.008	0.045±0.008	0.041±0.008	0.058±0.019	-

(C.2) Instantaneous influence F values (mean ± SE across subjects)

F(x.y)	rFIC	ACC	rDLPFC	rPPC	VMPFC	PCC
rFIC	-	0.253±0.034	0.127±0.021	0.080±0.017	0.088±0.018	0.081±0.019
ACC	x	-	0.193±0.027	0.117±0.019	0.100±0.017	0.236±0.045
rDLPFC	x	x	-	0.240±0.048	0.064±0.014	0.172±0.023
rPPC	x	x	x	-	0.030±0.007	0.099±0.025
VMPFC	x	x	x	x	-	0.140±0.027
PCC	x	x	x	x	x	-

(A.1, B.1, C.1) GCA directed influence terms $F_{x\to y}$ and $F_{y\to x}$ (mean ± SE, between pairs of regions across subjects). Influences are from column ROI to row ROI. Violet boxes indicate significant directed interactions, where the difference-of-influence term ($F_{x\to y}$ - $F_{y\to x}$) was significantly different from a bootstrap distribution at the group-level (Mann–Whitney U test, $P < 0.05$). The p-values (for significant $F_{x\to y}$ - $F_{y\to x}$) are reported within parenthesis inside the violet boxes; those p-values that survived an FDR correction ($q < 0.05$) for multiple comparisons are highlighted in blue (values indicated as 0.0000 refer to $P < 10^{-4}$).
(A.2, B.2, C.2) GCA instantaneous influence terms, $F_{x.y}$ (mean ± SE, between pairs of regions across subjects; the matrix is symmetric, so only upper triangular elements are shown). Red boxes indicate the optimal cluster configuration corresponding to a pairing of regions that maximizes sum of mutual instantaneous influences, $\Sigma F_{x.y}$. Across all tasks, the optimal pairs were identical with the SN (rFIC, ACC), CEN (rDLPFC, rPPC) and DMN (VMPFC, PPC).

Table S5. Network analysis of the causal interactions in the three experiments

ROI	Out-degree	In-degree	Out-In degree	Path length
		A. Auditory event segmentation		
rFIC	**3.00 ± 0.26**	**1.05 ± 0.18**	**+1.95 ± 0.38**	**1.22 ± 0.06**
ACC	1.15 ± 0.28	1.99 ± 0.30	−0.84 ± 0.53	1.44 ± 0.07
rDLPFC	1.06 ± 0.26	2.09 ± 0.24	−1.02 ± 0.46	1.41 ± 0.05
rPPC	1.24 ± 0.30	1.72 ± 0.31	−0.49 ± 0.55	1.47 ± 0.08
VMPFC	2.01 ± 0.33	1.52 ± 0.24	+0.49 ± 0.53	1.36 ± 0.07
PCC	1.57 ± 0.31	1.66 ± 0.31	−0.09 ± 0.53	1.49 ± 0.12
		B. Visual ″oddball″ attention		
rFIC	**1.86 ± 0.39**	**0.72 ± 0.24**	**+1.14 ± 0.54**	**1.61 ± 0.15**
ACC	0.94 ± 0.29	0.92 ± 0.29	+0.02 ± 0.49	1.87 ± 0.19
rDLPFC	0.49 ± 0.16	1.54 ± 0.34	−1.05 ± 0.36	1.68 ± 0.11
rPPC	0.87 ± 0.24	0.95 ± 0.23	−0.08 ± 0.35	2.06 ± 0.35
VMPFC	0.85 ± 0.29	0.87 ± 0.30	−0.02 ± 0.42	2.00 ± 0.24
PCC	0.67 ± 0.36	0.68 ± 0.23	−0.01 ± 0.47	1.93 ± 0.13
		C. Task-free resting state		
rFIC	**2.50 ± 0.25**	**0.81 ± 0.17**	**+1.70 ± 0.36**	**1.40 ± 0.07**
ACC	1.10 ± 0.23	1.53 ± 0.25	−0.43 ± 0.42	1.53 ± 0.05
rDLPFC	0.99 ± 0.28	1.56 ± 0.26	−0.57 ± 0.47	1.53 ± 0.07
rPPC	1.13 ± 0.25	1.24 ± 0.22	−0.11 ± 0.41	1.79 ± 0.24
VMPFC	1.05 ± 0.20	1.55 ± 0.21	−0.50 ± 0.33	1.62 ± 0.09
PCC	1.41 ± 0.31	1.49 ± 0.31	−0.08 ± 0.56	1.54 ± 0.12

Network analysis on the causal interactions identified with GCA revealed that the rFIC (boldface) had the highest out-degree, lowest in-degree, highest out-in degree, and shortest path length among all regions of the SN, CEN, and DMN. This indicates that the rFIC is a critical outflow hub at the intersection of the CEN and DMN.
Out-degree: Number of causal outflow connections from a node
In-degree: Number of causal in-flow connections to a node
Out-In-degree: Difference between ″Out-degree″ and ″In-degree″ (a measure of net causal outflow from a node)
Path length: Shortest path from a node to every other node in the network calculated by Dijkstra's algorithm (normalized by the number of nodes minus one).
Values of the metrics reported are mean ± SE across subjects.